LA-UR-91- 91-3091

LA-UR--91-3091

DE92 000179

Los Alamos National Laboratory is operated by the University of California for the United States Department of Energy under contract W-7405-ENG-36

TITLE: **PHYSICS DESIGN OF THE HIGH BRIGHTNESS LINAC FOR THE ADVANCED FREE-ELECTRON LASER INITIATIVE AT LOS ALAMOS**

AUTHOR(S): Richard L. Sheffield, M. Jean, Browman, Bruce E. Carlsten, and Lloyd M. Young

SUBMITTED TO: Thirteenth International Free-Electron Laser Conference
Santa Fe, NM
August 25-30, 1991

DISCLAIMER

Los Alamos
Los Alamos National Laboratory
Los Alamos, New Mexico 87545

FORM NO. 836 R4
ST NO 2629 5/81

Physics Design of the High Brightness LINAC for the Advanced Free-Electron Laser Initiative at Los Alamos*

R. L. Sheffield, M. J. Browman, B. E. Carlsten, and L. M. Young
Los Alamos National Laboratory
Los Alamos, NM 87545

Abstract

Free electron lasers and high energy physics accelerators have increased the demand for very high brightness electron beam sources. This paper describes the design of an accelerator which can produce beams of greater than 7 x 10^{11} A/m^2 (brightness = 2*I/ε^2, with ε = 90% normalized emittance = 4 * rms emittance). The beam emittance growth in the accelerator is minimized by the following: producing a short electron bunch in a high gradient rf cavity, using a focusing solenoid to correct the emittance growth due to space charge, and designing the coupling slots between accelerator cavities to minimize quadruple effects. The simulation code PARMELA was modified for this design effort. This modified version uses SUPERFISH output files for the accelerator cavity fields, MAFIA output files for the 3-D perturbation fields due to the coupling slots in the accelerator cells, and POISSON output files for the solenoid field in the gun region. The results from simulations are, at 2.3 nC, a peak current of 180 A and a 90% emittance of 6.4 π mm-mrad, and, at 4.6 nC, a peak current of 300 A and a 90% emittance of 9.4 π mm-mrad. The exit energy from the linac is 20 MeV for both cases. A magnetic pulse compressor can be used to further increase the peak current.

Introduction

A new accelerator design that produces a very bright electron beam in a compact form has been developed through the Advanced Free-Electron Laser Initiative[1] (AFELI) at Los Alamos National Laboratory. The AFELI has the goal of building a second-generation FEL. This FEL will be designed to be suitable for a wide range of industrial, medical, and research applications. State-of-art components will be incorporated so that the FEL system will be compact in size, robust, and user friendly.

The accelerator design incorporates the experience gained from the initial photoinjector experiments[2] and the later accelerator experiments at APEX[3]. The design simulations were performed using a modified version of the code PARMELA.

For this paper, we use the 90% normalized emittance, ε_n, equivalent to 4 times

the rms value. Thus,

$$\varepsilon_n(90\%) = \beta\gamma\varepsilon_x = 4\pi\beta\gamma[\langle x^2\rangle\langle x'^2\rangle - \langle x\cdot x'\rangle^2]^{1/2},$$

where γ is the relativistic factor, β is the particle velocity divided by the speed of light, x is transverse beam size, x' transverse beam divergence, and ε_x is the unnormalized emittance.

The emittance is calculated in two ways. The "full" emittance is the usual emittance calculation for the entire micropulse in time and space. The "slice" emittance is calculated by the following. A micropulse is divided into slices in time equal to a slippage length. To insure enough particles are in a slice to give reasonable statistics, the smallest time slice is limited to 1% of the total pulse length. The reason for calculating the slice emittance is that electrons do not generate gain over the entire pulse, but only for the middle portion (in time) of the pulse. The use of slice emittance is invalid if temporal mixing occurs. With mixing, the full rms emittance must be used. To minimize mixing and to preserve beam brightness, great care must be given to proper beamline design[4].

Overall Accelerator Design

The design goals for the accelerator are to maximize beam brightness, use a simple design, and be capable of relatively high duty factor (0.1%) operation. The design point is > 2 nC charge per micropulse and an effective emittance of less than 10 π mm-mrad. Simple design is accomplished by using a single rf feed to drive the entire accelerator structure. The accelerator (Fig. 1) design is: 20 MeV output energy, average cavity gradients of 22 MeV/m, up to 20 Hz repetition rate, up to 50 μs long macropulses, 8 to 20 ps long micropulses, and liquid nitrogen operation. The accelerator operates with a 1300 MHz, 20 MW peak power klystron. For more details on the accelerator's engineering design see ref 1.

Compensating Emittance Growth due to Space Charge by using a Solenoid

The use of a solenoid to reduce emittance growth due to space charge has been discussed in several papers.[5] A representative configuration is shown in Fig. 2. At the cathode, the electron bunch emittance is determined by the cathode's thermal emittance (position 1 in Fig. 2). As an electron bunch leaves the cathode, the bunch expands radially due to space charge. Since the space charge force acts continuously on the bunch, no single discrete lens can compensate for the distortion of the distribution in phase space (position 2 in Fig. 2). However, a simple lens can be used to focus the bunch (position 3 in Fig. 2). Then, to first order, the same forces that acted on the bunch during expansion are present while the bunch is focused (position 4 in Fig. 2). Thus, the emittance growth that has occurred can be significantly reduced by proper lens placement. A unique solenoid design follows from the requirements of minimum emittance growth and simultaneously having the beam focused at a particular axial location. The solenoid design depends on the accelerator gradient, current density, and location of the peak magnetic field with respect to the cathode. The emittance numbers in Fig. 2 are from a typical PARMELA run. To be able to accurately render the solenoid field profiles, we incorporated the POISSON field maps of the solenoid directly into a modified version PARMELA.

From simulations, we computed the effect on the final emittance due to the cathode thermal effects. As expected, the final emittance is the sum of squares of the final emittance calculated with zero cathode temperature and the finite cathode emittance. An example is shown in Fig. 2.

Minimizing Perturbations due to Accelerator Coupling Slots

The APEX accelerator[3] was the first more than two cell photoinjector design. The standing-wave, 1300 MHz, π-mode accelerator is designed with on-axis coupling slots. The initial PARMELA simulations gave a symmetrical beam at the accelerator exit (Fig. 3). IN the APEX experiment, however, the accelerator produced elliptical beams. By incorporating MAFIA field maps due to the coupling slots into PARMELA, we found that the coupling slots produced a quadruple lens in every accelerator cell. A sample output plot of the APEX photoinjector from the modified PARMELA is shown in Fig. 4.

Several possible types of on-axis coupling are shown in Fig. 5. The effect of coupling slots is significant for very high brightness beams. A single slot produces a dipole lens, two slots produce a quadruple lens, four slots gives an octupole, and so on. Each accelerator cell (except the cells at the accelerator ends) has coupling slots on

each half an accelerator cell. The relative orientation of the slots on either end of the cell will determine the relative angle of the corresponding lens. The two coupling slot configuration gives a quadruple lens at the entrance and exit of the accelerator cell, respectively. The orientation of the slots will determine whether the quadruple lens add or subtract for each cell. In the APEX arrangement (type H) the fields for each cell added, giving a net quadruple lens. In a type T arrangement the fields subtract, giving a net effect close to zero.

The cancellation of the quadruple effects in a type T arrangement is nearly zero only for a highly relativistic beam. In the first few cells, where the beam is still not highly relativistic, a net quadruple lens still exists. Figure 6 shows the beam's phase space and spatial profile using type T coupling cells throughout the accelerator. The figure shows an unsymmetrical beam at the exit of the accelerator.

The coupling slot design for the AFEL accelerator uses a four coupling slot arrangement for the first two cells and a type T configuration for the remaining accelerator cells. Since the four slot arrangement has no quadruple component, then the first two cells produce no beam asymmetry. After the beam exits the first two cells the beam is highly relativistic and the type T coupling gives a very small net quadruple focusing. This configuration is shown in Fig. 7. The PARMELA simulation for Fig. 7 is shown in Fig. 8.

The four coupling slot arrangement cannot be carried throughout the accelerator. At the high average currents of the AFEL, beam breakup will occur due to the coupling of a dipole mode from cell to cell. In the type T and H coupling cell configuration the dipole mode does not couple because the coupling slots are rotated 90° ~~degrees~~ in the coupling cavity. In the 4 slot coupling cells, the slots are rotated 45° ~~deg~~ in the coupling cavity which very effectively couples the dipole modes.

Other features of the AFEL accelerator

The first cell, a half-cell, is 9 mm longer than one-half of a standard 1300 Mhz cell. There are two advantages to a longer injection cell. First, the exit phase of the electron bunch depends on the cell length. Since the AFEL linac has a single rf feed, the proper operating phase to minimize energy spread was met by adjusting the first cell length. (If the minimum energy spread is outside the phase tuning range, a passive cavity following the linac will be used to minimize energy spread). Second, a longer first cell increases the electron beam energy at the exit of the first cell. This reduces the space charge effects and helps improve the final emittance. The exit energy from

the first cell is 1.5 MeV instead of 1.0 MeV for a regular half-cell.

Other engineering features of the AFEL accelerator are: capability of operation at 77K, UHV design, and high Q, high-gradient, long macropulse accelerator cells.

Beam dependencies

This type of accelerator is unique in that the electron beam distribution does not mix longitudinally. With no mixing, the rms emittance calculation for the full pulse underestimates the FEL performance. Figure 9 shows the x and y slice emittance during a micropulse for a gaussian and a square pulse. Except for statistical noise due to the limited number of particle in the simulation, the slice emittance is time independent during the micropulse. However, the emittance of the full pulse is significantly larger. The larger full pulse emittance is due to the variation in divergence throughout the micropulse (see upper graph in Fig. 10). Two factors help determine FEL performance: first, the local beam conditions in the micropulse (since the slippage length is a small fraction of the entire pulse length); second, the ability to match into the gain profile of the wiggler. Figure 10 shows the beam conditions that affect FEL performance. The upper two graphs are the beam divergence and the particle density as a function of time. The lower graph is a calculation of $\Delta\nu^6$ (gain width for a sample wiggler) as a function of time. The three graphs show that most of the electrons are in the gain width of the wiggler for the middle portion of a micropulse. The beginning and end of the micropulse are not matched into the wiggler, but the fraction of the electrons in the temporal wings is small. Again, this type of analysis is not correct if the beam mixes longitudinally.

The AFEL is designed to minimize components and distances to increase reliability and ease of use. However, the performance of the FEL design does depend strongly on a few parameters. The parameters that must be tightly controlled are: the radius of the cathode, the magnitude of the solenoid field around the cathode region, the accelerator phase, and the magnitude of the accelerator fields.

Engineering Issues

The choice of photocathode depends on the duty factor and pulse structure required for the application of the electron beam. At present, photocathodes fall into two categories: low quantum efficiency (QE) and high QE. The low QE cathodes typically have QEs less than 0.1% but are tolerant of the vacuum conditions in the

accelerator. The high QE cathodes have QEs greater than 1% but require an ultra-high vacuum environment. Thus for short pulse machines or low duty factors (<0.1%) low QE cathodes are acceptable. If the machine duty factor is greater than 1% than the high cost of average laser power constrains the choice of cathodes to high QEs.

Field emission from the cathode depends on the surface properties and gradient present in the cathode cell. Designs of high duty factor machines or experiments where the background charge levels are important must include the effect of the field emission. The field emission can occur either directly from or near the photocathode. Thus the maximum cell gradient might be limited, impacting the beam emittance. High QE cathodes seem to exhibit more field emission than the low QE cathodes.

The spatial profile of the photocathode laser and photocathode QE are important. In general, spatial profiles in which the electron density decreases with radius, as opposed to radially uniform or slightly increasing with radius, produce a greater emittance.

To preserve a bright electron beam throughout the beamline requires detailed simulations. The AFEL beamline was designed[4] and the parametric sensitivities measured[7] using PARMELA.

Finally, the rf power and the photocathode laser must be stable. The stability requirements in phase in amplitude depend on the application. Present laser stability measurements[8] are <0.5 ps and <1% amplitude variations.

Results

The following results are based on the performance of the FEL using the slice emittance as opposed to the integrated emittance of the entire micropulse. This implies that the contribution of the temporal tails of the micropulse are ignored. The results are:

- The largest component of the emittance is due to the variation of the radial velocity during the micropulse and is correlated.
- The next largest component of the emittance is due to radial rf effects.
- A gaussian pulse in time gives almost the same performance as a square pulse in time.
- A micropulse of 2.3 nC has a slice emittance less than 6 π mm-mrad, a peak current greater than 175 A, and an effective energy spread of less than 0.3%.
- A micropulse of 4.6 nC has a slice emittance less than 10 π mm-mrad, a peak current greater than 310 A, and an effective energy spread of less than 0.3%.

Simulations show that visible wavelength operation (>50% gain @ 400 nm) is possible using a low energy (20 MeV), high-gradient (>20 MeV/m) accelerator.

Conclusion

This paper described the design of an accelerator which can produce beams of greater than 7×10^{11} A/m^2 (brightness = $2^*I/\varepsilon^2$, with ε = 90% normalized emittance). The design presented shows that beam emittance growth in the accelerator can minimized by careful design of the accelerator. The results from simulations are, at 2.3 nC, a peak current of 180 A and a 90% slice emittance of 6.4 π mm-mrad, and, at 4.6 nC, a peak current of 300 A and a 90% slice emittance of 9.4 π mm-mrad. The exit energy from the linac is 20 MeV for both cases.

Figure 1. AFEL linac schematic. Dimensions are in inches.

Figure 2. Placing a solenoid near the cathode can compensate for space charge emittance growth. Position 1 is at the cathode. Position's 2 and 3 are before and after the solenoid center (with the center between 5 and 15 cm from the cathode). Position 4 is downstream of the accelerator. The figure also shows the growth in emittance (6 π mm-mrad) above the thermal emittance (5 π mm-mrad) present at the cathode.

Figure 3. PARMELA simulation result neglecting the effects of coupling fields.

Figure 4. PARMELA simulation result with the type H coupling cell configuration.

Figure 5. Possible coupling slot arrangements with four and two slot coupling. CS is a coupling cell. AC is an accelerator cell.

Figure 6. PARMELA simulation result with the type T coupling cell configuration.

Figure 7. The AFEL coupling slots and accelerator cells arrangement.

Figure 8. PARMELA simulation result for the AFEL accelerator.

Figure 9. Plots of the slice emittance during a micropulse. The plots give results for pulses which are either gaussian or square in time. The bottom graph compares the 90% emittance and the middle of the pulse emittance.

Figure 10. The upper plot shows the beam divergence during the pulse. The middle plot shows how well matched the pulse is to the gain profile of the wiggler.

---

[1] K. C. D. Chan et al., these proceedings, 91FEL.

[2] R. L. Sheffield, AIP Conf. Proc. 184, 2, 1500 (1988).

[3] P. G. O'Shea et al., these proceedings, 91FEL.

[4] T. F. Wang, K. C. D. Chan, R. L. Sheffield, and W. L. Wilson, these proceedings, 91FEL.

[5] B. E. Carlsten, Porc.10th Int. FEL conf, Jerusalem, Israel, 1988, Nucl. Instr. and Meth., A285 (1989) 313; B. E. Carlsten and R. L. Sheffield, Poc. 1988 Linac Conf. Williamsburg, Va, 1988, CEBAF Report 89-001 (1989) 365; B. E. Carlsten, Poc. 1989 IEEE Part. Accel. Conf., Chicago, IL, IEEE Catalog no. 89CH2669-0 (1989) 313.

[6] W. B. Colson, G. Dattoli, and F. Ciocci, *Phys Rev. A*, **64**,(1985), 2

[7] S. Hartmann, A. Lombardi, R. L. Sheffield, and T. Wang, these proceedings, 91FEL.

[8] J. Early, J. Barton, R. Wenzel, D. Remelius, and G. Busch, these proceedings, 91FEL

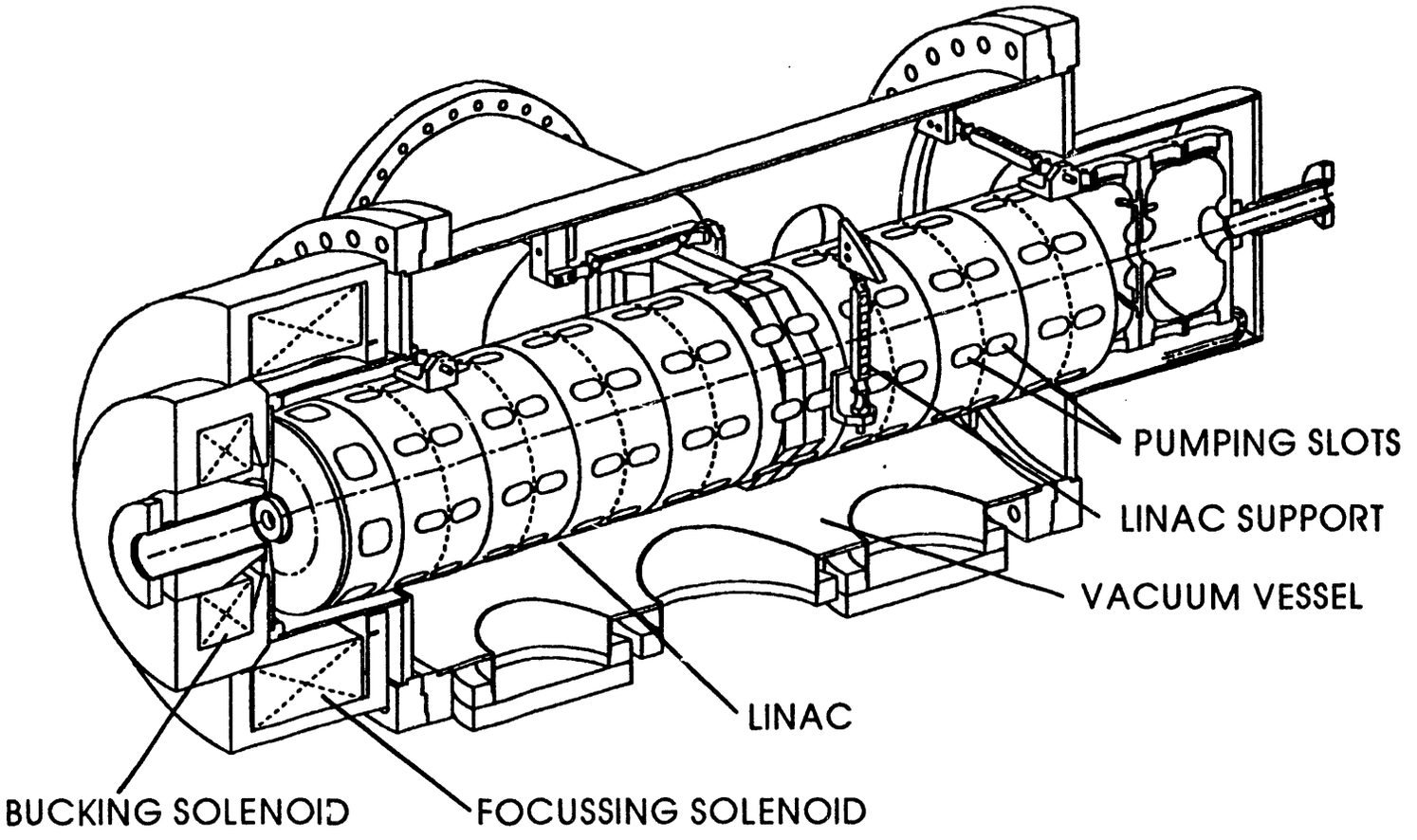
PUMPING SLOTS
LINAC SUPPORT
VACUUM VESSEL
LINAC
BUCKING SOLENOID
FOCUSSING SOLENOID

Fig 1

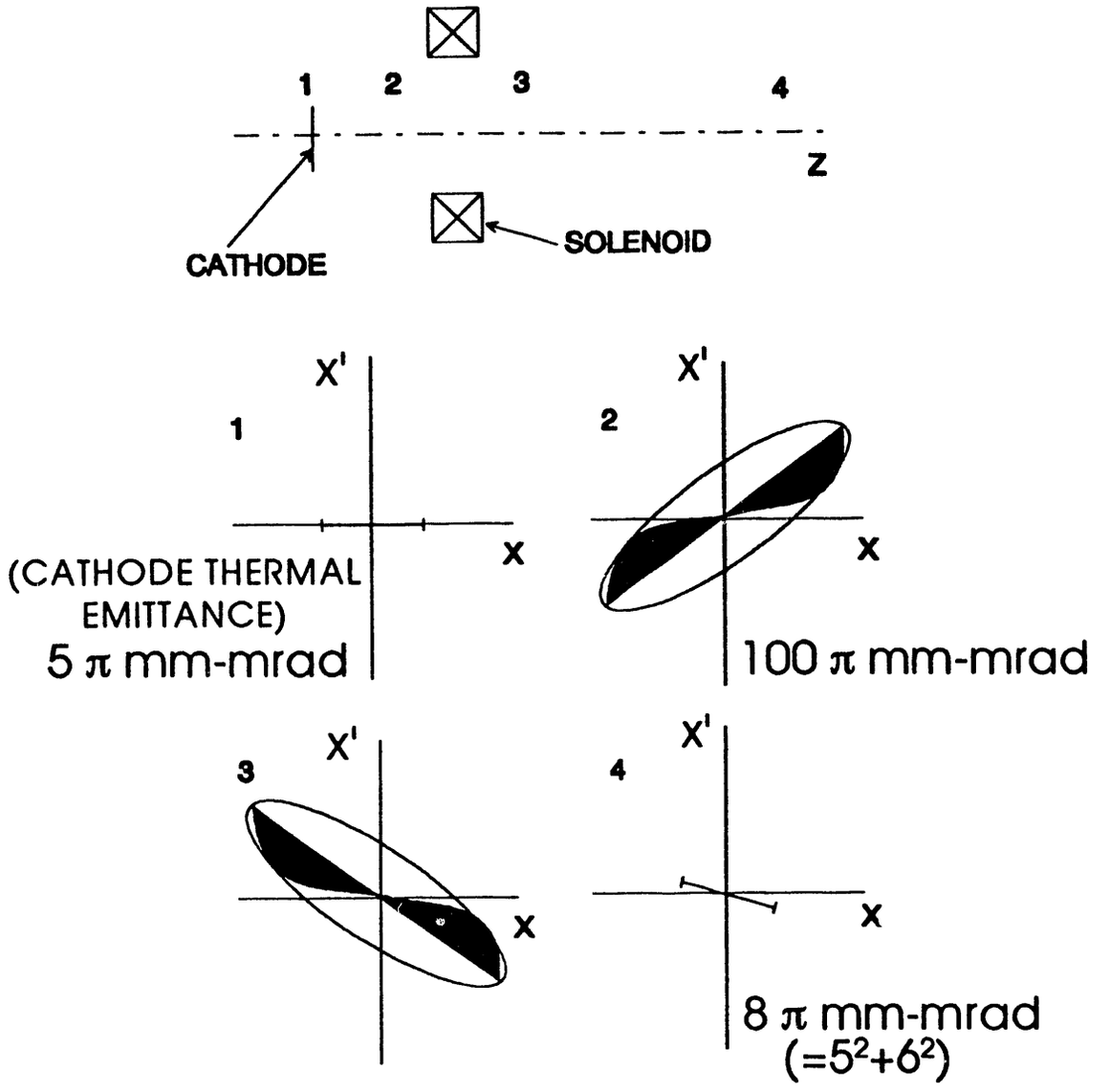
1
2
3
4
Z
CATHODE
SOLENOID
X'
1
X
(CATHODE THERMAL EMITTANCE)
5 π mm-mrad
X'
2
X
100 π mm-mrad
X'
3
X
X'
4
X
8 π mm-mrad
(=5²+6²)

Fig 2

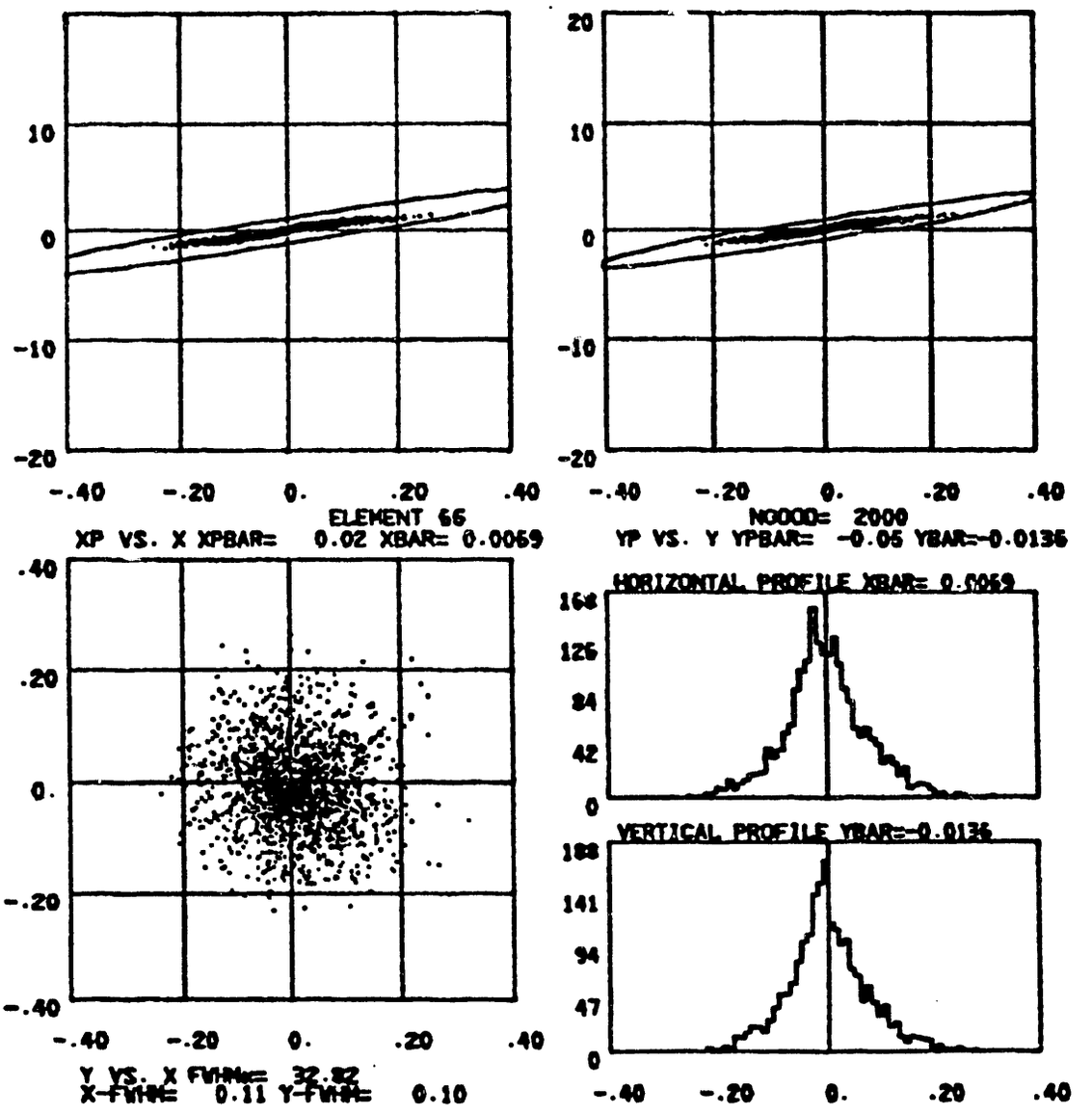
10
0
-10
-20
-.40
-.20
0.
.20
.40
ELEMENT 66
XP VS. X XPBAR= 0.02 XBAR= 0.0069
20
10
0
-10
-20
-.40
-.20
0.
.20
.40
NOOOO= 2000
YP VS. Y YPBAR= -0.05 YBAR=-0.0136
.40
.20
0.
-.20
-.40
-.40
-.20
0.
.20
.40
Y VS. X FWHM= 32.82
X-FWHM= 0.11 Y-FWHM= 0.10
HORIZONTAL PROFILE XBAR= 0.0069
168
126
84
42
0
VERTICAL PROFILE YBAR=-0.0136
188
141
94
47
0
-.40
-.20
0.
.20
.40

Fig. 3

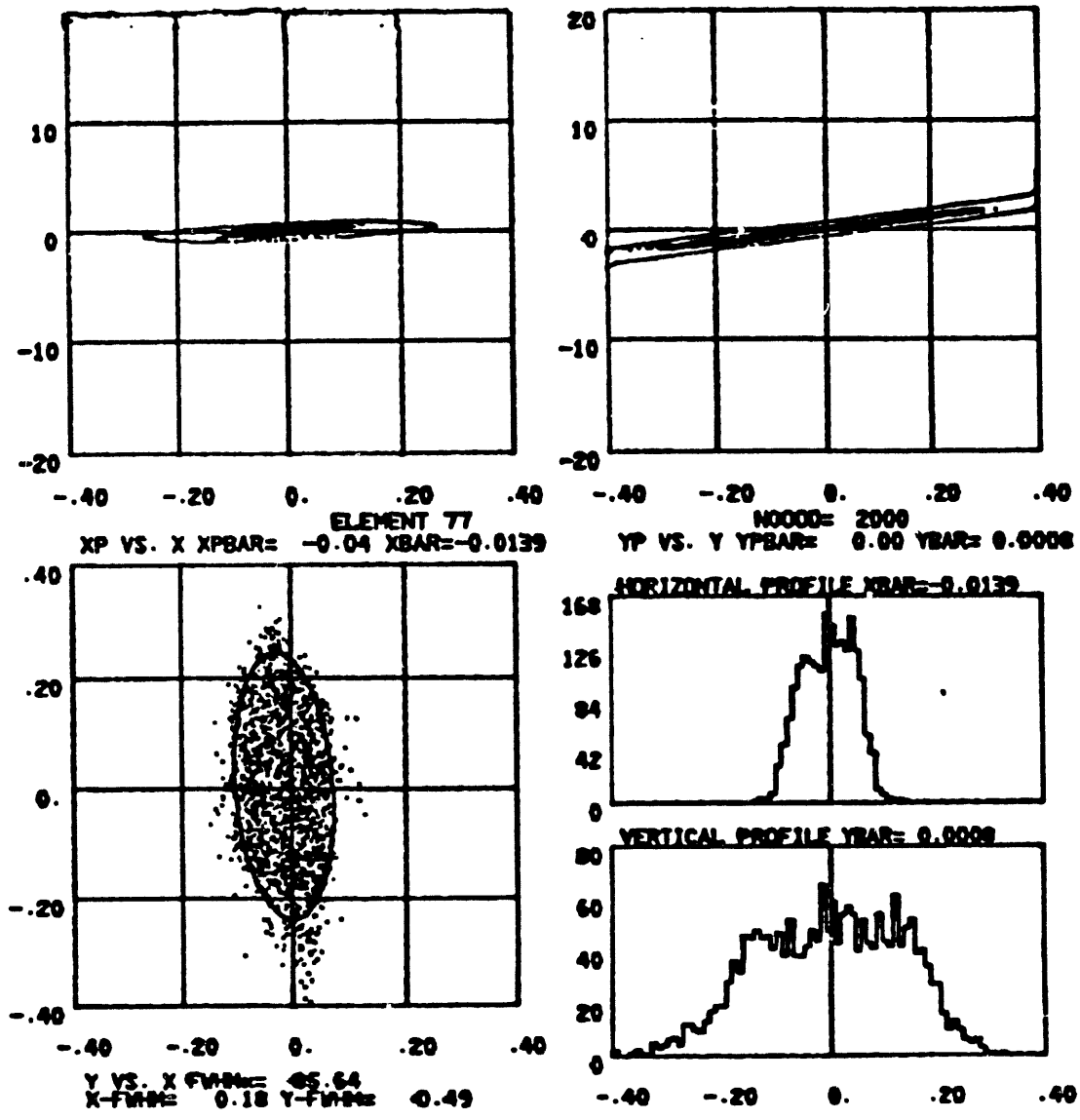
10
0
-10
-20
-.40
-.20
0.
.20
.40
ELEMENT 77
XP VS. X XPBAR= -0.04 XBAR=-0.0139
20
10
0
-10
-20
-.40
-.20
0.
.20
.40
NOOOO= 2000
YP VS. Y YPBAR= 0.00 YBAR= 0.0008
.40
.20
0.
-.20
-.40
-.40
-.20
0.
.20
.40
Y VS. X FWHM= 85.64
X-FWHM= 0.18 Y-FWHM= 0.49
HORIZONTAL PROFILE XBAR=-0.0139
168
126
84
42
0
VERTICAL PROFILE YBAR= 0.0008
80
60
40
20
0
-.40
-.20
0.
.20
.40

Fig. 4

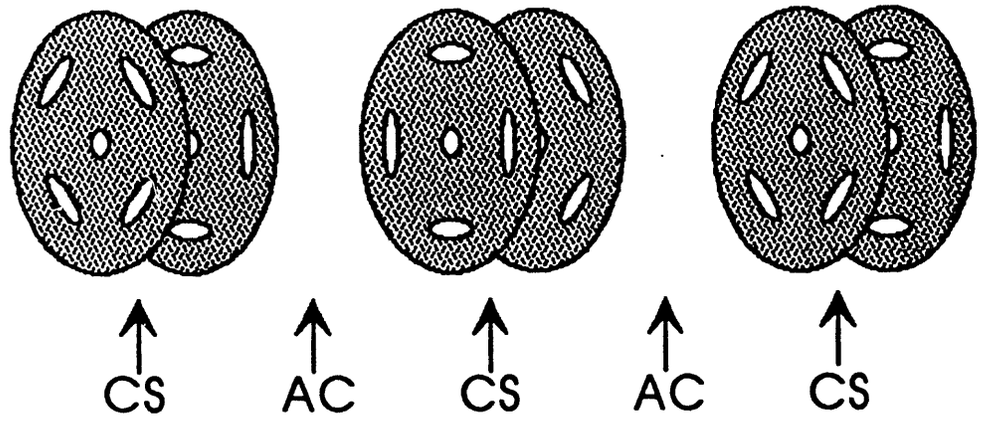

'4' - FOUR SLOTS ON AN END WALL

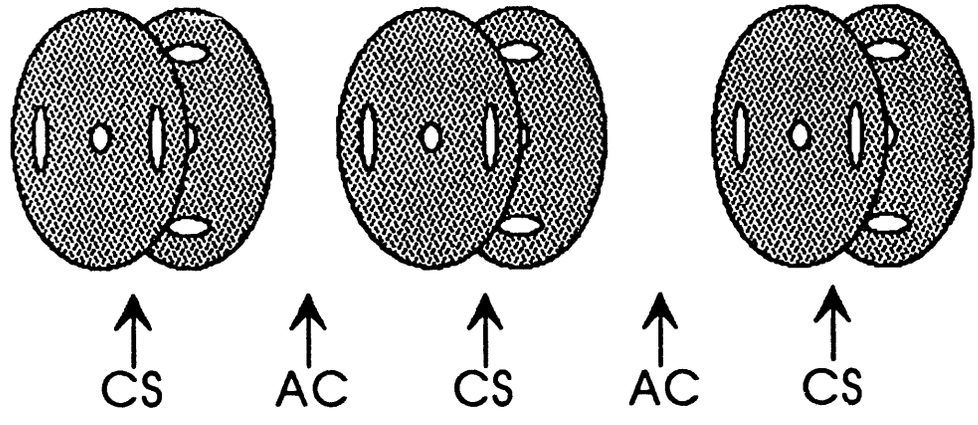

'H' - SLOT ARRANGEMENT

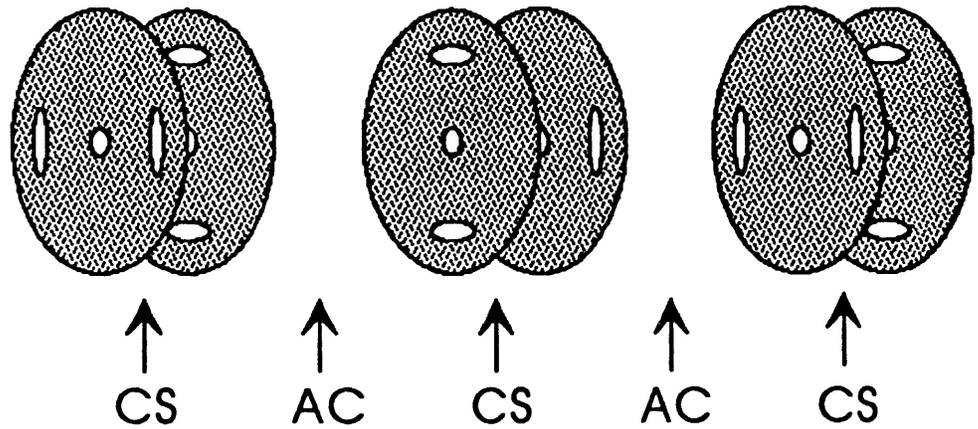

'T' - SLOT ARRANGEMENT

Fig. 5

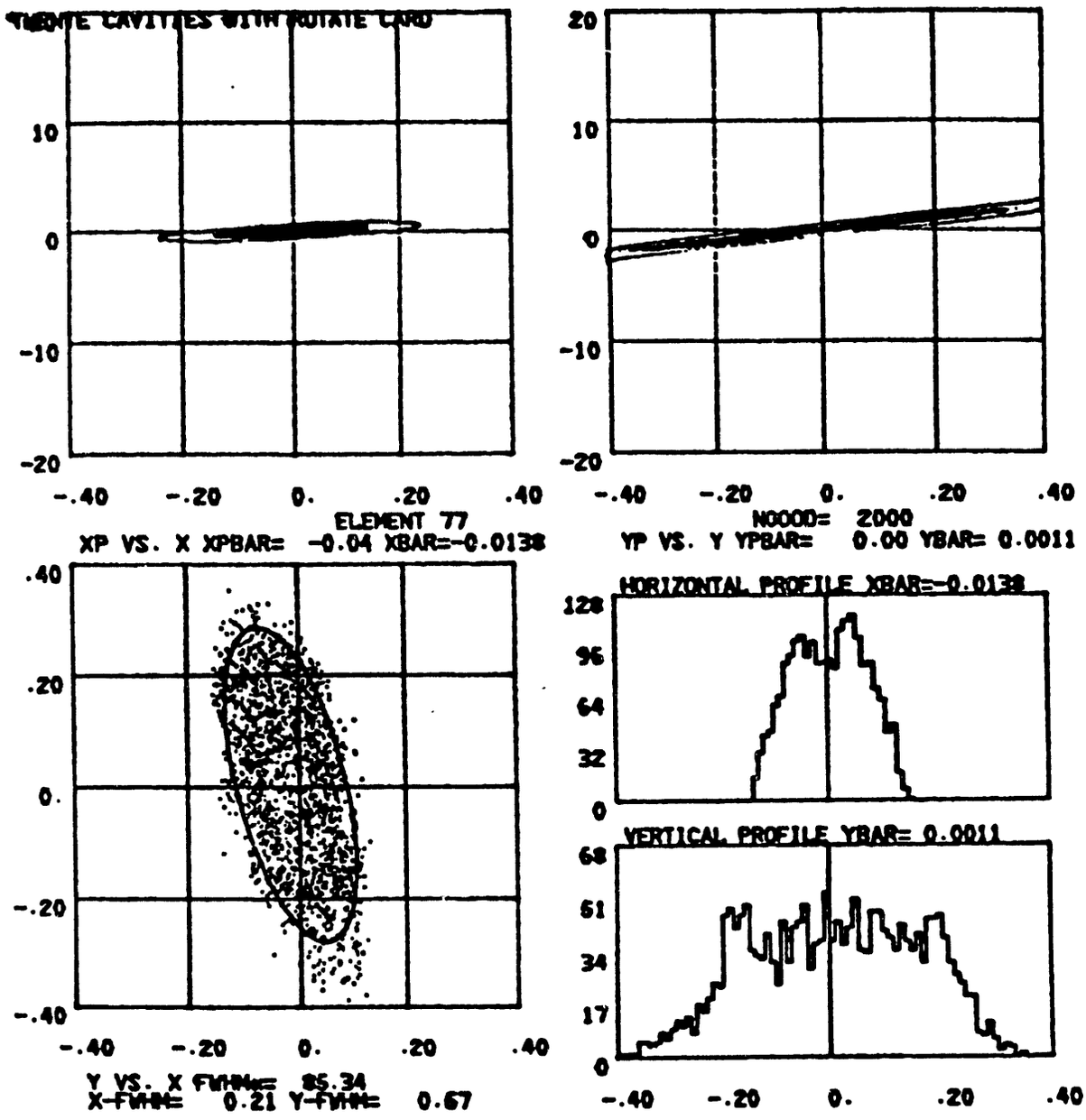
20
10
0
-10
-20
-.40
-.20
0.
.20
.40
ELEMENT 77
XP VS. X XPBAR= -0.04 XBAR=-0.0138
NOOOD= 2000
YP VS. Y YPBAR= 0.00 YBAR= 0.0011
HORIZONTAL PROFILE XBAR=-0.0138
128
96
64
32
VERTICAL PROFILE YBAR= 0.0011
68
51
34
17
Y VS. X FWHM= 85.34
X-FWHM= 0.21 Y-FWHM= 0.67

Fig. 6

1300 MHz ADVANCED FEL LINAC
COUPLING SLOT ARRANGEMENT

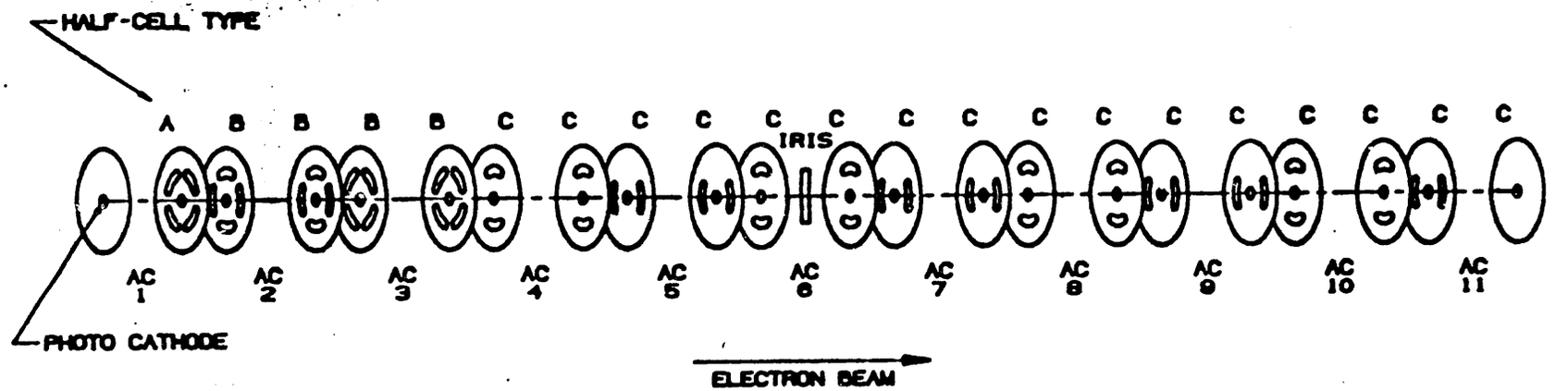

LOS ALAMOS NATIONAL LABORATORY
LOS ALAMOS NEW MEXICO
GROUP AT-1

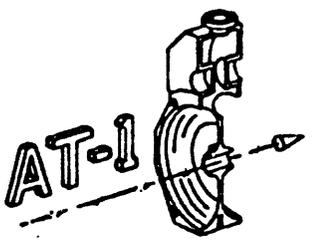

JAN. 10, 1991

Fig 7

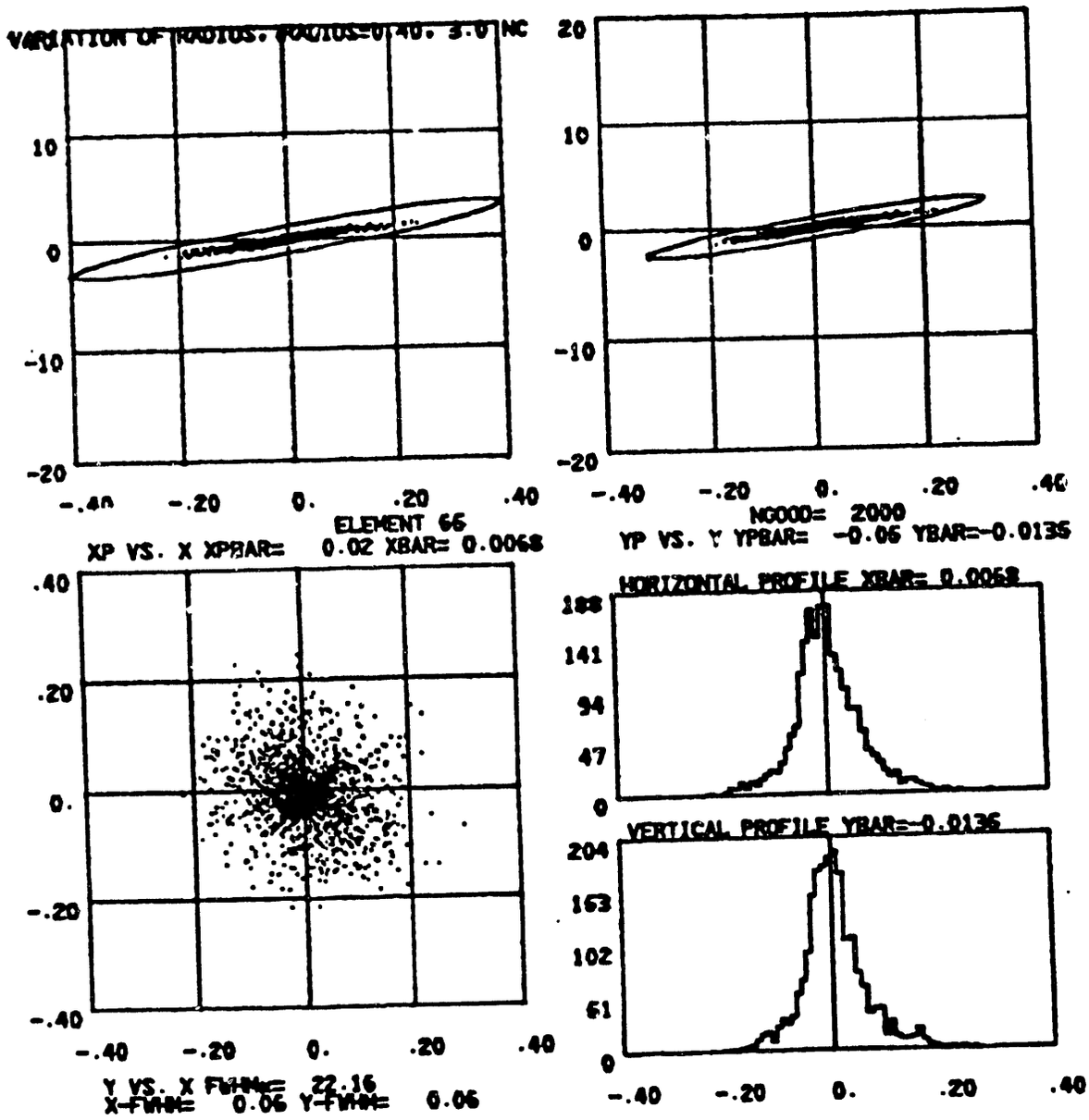
VARIATION OF RADIUS: RADIUS=0.40: 3.0 NC
10
0
-10
-20
-.40
-.20
0.
.20
.40
20
NGOOD= 2000
YP VS. Y YPBAR= -0.06 YBAR=-0.0135
ELEMENT 66
XP VS. X XPBAR= 0.02 XBAR= 0.0068
.40
.20
0.
-.20
-.40
Y VS. X FWHM= 22.16
X-FWHM= 0.06 Y-FWHM= 0.06
HORIZONTAL PROFILE XBAR= 0.0068
188
141
94
47
0
VERTICAL PROFILE YBAR=-0.0136
204
153
102
51
0

Fig. 8

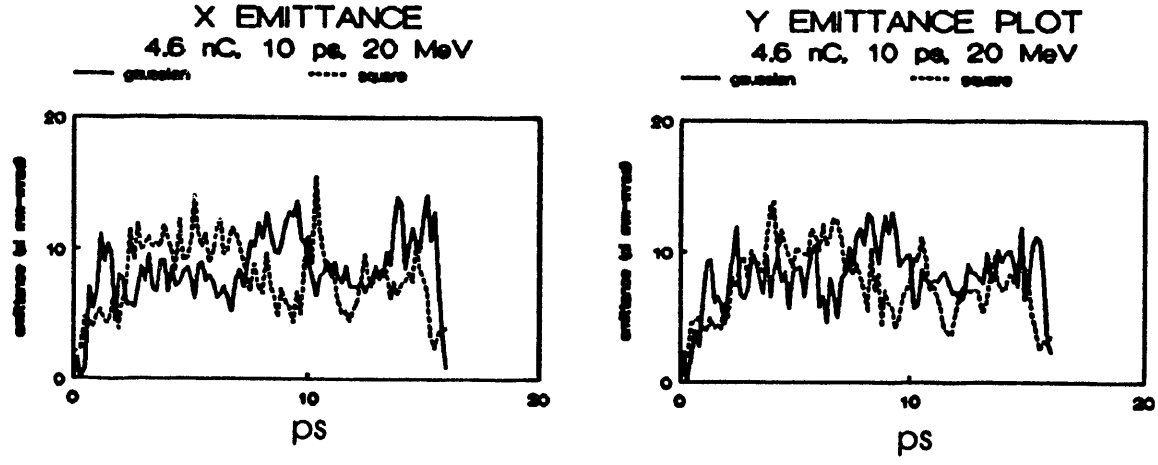
X EMITTANCE
4.6 nC, 10 ps, 20 MeV
gaussian
square
20
10
0
0
10
20
ps
Y EMITTANCE PLOT
4.6 nC, 10 ps, 20 MeV
gaussian
square
20
10
0
0
10
20
ps

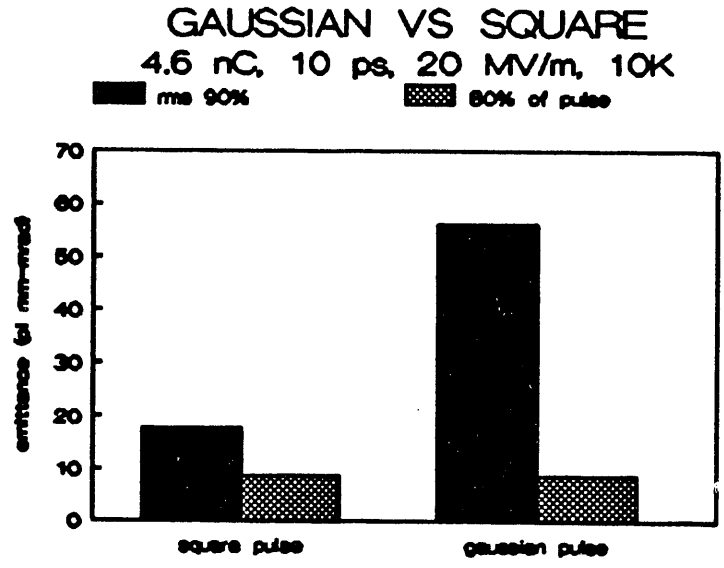
GAUSSIAN VS SQUARE
4.6 nC, 10 ps, 20 MV/m, 10K
rms 90%
80% of pulse
70
60
50
40
30
20
10
0
square pulse
gaussian pulse

Fig.9

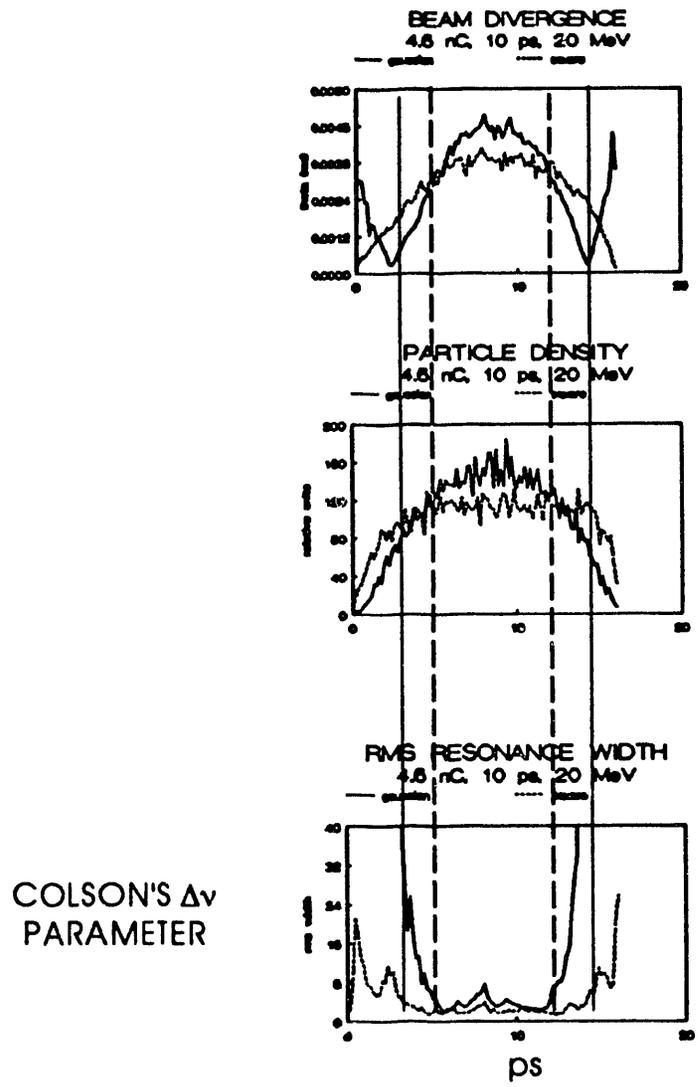
BEAM DIVERGENCE
4.6 nC, 10 ps, 20 MeV
PARTICLE DENSITY
4.6 nC, 10 ps, 20 MeV
RMS RESONANCE WIDTH
4.6 nC, 10 ps, 20 MeV
COLSON'S Δv
PARAMETER
ps

Fig. 10

END

DATE FILMED

10/28/91